A defect in skeletal muscle sodium channel deactivation exacerbates hyperexcitability in human paramyotonia congenita

David E. Featherstone, Esther Fujimoto and Peter C. Ruben

Department of Biology, Utah State University, Logan, UT 84322-5305, USA

(Received 6 May 1997; accepted after revision 30 September 1997)

1. Paramyotonia congenita (PC) is a human hereditary disorder wherein missense mutations in the skeletal muscle sodium channel lead to cold-exacerbated muscle hyperexcitability. The most common site for PC mutations is the outermost arginine of domain IV segment 4 (human R1448, rat R1441).

2. We examined the rat homologues of two PC mutants with changes at this site: R1441P and R1441C. The R→P mutation leads to the most clinically severe form of the disease. Since PC has so far been attributed to defects in fast inactivation, we expected the R→P substitution to have a more dramatic effect on fast inactivation than R→C. Both mutants (R1441P and R1441C), however, had identical rates and voltage dependence of fast inactivation and activation.

3. R1441P and R1441C also had slowed deactivation, compared with wild-type, raising the possibility that slowed deactivation, in combination with defective fast inactivation, might be a contributing cause of paramyotonia congenita. Furthermore, deactivation was slower in R1441P than in R1441C, suggesting that the worse phenotype of the human R→P mutation is due to a greater effect on deactivation, and supporting our hypothesis that slowed sodium channel deactivation contributes to paramyotonia congenita.

4. We show that the downstroke of the muscle action potential produced a sodium tail current, and thus slowed deactivation opposes repolarization and therefore leads to hyperexcitability. Hyperexcitability due to slowed deactivation, which has previously been overlooked, also predicts the temperature sensitivity of PC, which has otherwise not been adequately explained.

Several genetic muscle diseases, such as periodic paralyses and inherited cardiac arrhythmia, are a result of mutations in muscle ion channels (Schwartz *et al.* 1995; Wang *et al.* 1995*b*; Cannon, 1996; Ptacek & Griggs, 1996). In each of these diseases, malfunctions in ion channel gating lead to destabilized membrane potentials and subsequent muscle hyperexcitability. In cases wherein the diseases have been specifically shown to result from mutations in sodium channels, the phenotype has been most commonly attributed to defects in fast inactivation (Chahine, 1994; Yang *et al.* 1994; Hayward, Brown & Cannon, 1996). These defects are thought to lead to hyperexcitability and therefore paralysis (in the case of the periodic paralyses) or a lengthened cardiac action potential and predisposition towards fatal arrhythmia (in the case of cardiac long-QT syndrome) (Bennet, Yazawa, Makita & George, 1995).

Inherited 'channelopathies' (Zhou, Spier & Hoffman, 1994) such as these provide an opportunity to correlate channel biophysics and *in vivo* function. For example, the mutations associated with paramyotonia congenita (PC), an autosomal dominant human muscle disorder (Ptacek & Griggs, 1996), result in temperature-exacerbated, uncontrollable muscle tension after contraction (Rudel & Lehmann-Horn, 1985; Lehmann-Horn, Rudel & Ricker, 1987). This tension is due to muscle fibre membrane hyperexcitability that produces long bursts of action potentials ('myotonic runs'; Rudel & Lehmann-Horn, 1985) rather than one or only a few spikes in response to a motor neuron discharge.

The most common location for skeletal muscle sodium channel mutations that result in paramyotonia congenita is amino acid position 1448. In human wild-type (WT) voltage-gated skeletal muscle sodium channels, this position is occupied by an arginine, and serves as part of the S4 'voltage sensor' in domain IV (George, Komisarof, Kallen & Barachi, 1992). In paramyotonia congenita, a missense mutation results in the substitution of a histidine, cysteine or proline. The Arg→Pro mutation is particularly interesting since it causes the most clinically severe and cold-sensitive phenotype, compared with Arg→Cys and Arg→His (Wang, Dubowitz, Lehmann-Horn, Ricker, Ptacek & Hoffman, 1995*a*).

In this study, the biophysics of the Arg→Pro and Arg→Cys substitutions were compared by introduction of the equivalent mutations (R1441P and R1441C) into rat skeletal muscle sodium channels. Both mutations produced equivalent changes in fast inactivation (onset and recovery), as has been observed for all sodium channel myotonias (Chahine, 1994; Yang *et al.* 1994; Hayward *et al.* 1996). The voltage dependence of steady-state fast inactivation was also affected equally in both mutations, while no changes were detected in the voltage dependence of activation, compared with WT. R1441P differed only from R1441C by having slower deactivation. The physiological role of deactivation was investigated by examining sodium currents in response to an action potential-shaped voltage-command potential, revealing that the downstroke of an action potential resulted in a sodium 'tail current' that is accentuated in the fast-inactivation defective mutants. Based on this, and computer modelling, we concluded that slowed deactivation opposes repolarization following an action potential and therefore results in hyperexcitability. Since the greater severity (including cold sensitivity) of the Arg→Pro phenotype, compared with Arg→Cys, results solely from slower deactivation, the exacerbation of symptoms due to cold temperatures must also result from slowed deactivation. Muscle stiffness due to cold is a hallmark of paramyotonia congenita (Rudel & Lehmann-Horn, 1985; Lehmann-Horn *et al.* 1987; Sansone, Rotondo, Ptacek & Meola, 1994), yet this characteristic has never been sufficiently explained by observed channel biophysics. As a result of this study, we hypothesize that increasingly slowed deactivation, such as would occur with cooling, causes increasing opposition to fast membrane repolarization, and therefore that the temperature sensitivity of the disease may be due to slowing of deactivation in PC mutants, in combination with slowed fast inactivation. This work has been previously published in abstract form (Featherstone, Fujimoto & Ruben, 1997).

METHODS

Site-directed mutagenesis on rat SkM1 WT sodium channels in pGH19 (a gift from the laboratory of A. Goldin, University of California, Irvine, CA, USA; Trimmer *et al.* 1989) was performed using the polymerase chain reaction (PCR) overlap extension method (Ho, Hunt, Morton, Pullen & Pease, 1989). A 748 bp *Bst*I1071–*Sac*II fragment was removed from the rSkM1/pGH19 cloned cDNA. PCR fragments were made with synthetic oligo-nucleotides to introduce point mutations, digested with *Bst*I1071 and *Sac*II, then ligated back into the original clone. Oligonucleotide sequences were:

BstL: CAA CAA CAA GTC CGA GTC TGA G;
SacR: AGG AGG CCG ATG TTG AAG AG;
R1441CL: CTG TTC TGT GTG ATC CGC TTG;
R1441CR: CAC ACA GAA CAG CGT GGG TG;
R1441PL: CTG TTC CCT GTG ATC CGC TTG;
R1441PR: CAC AGG GAA CAG CGT GGG TG.

All amplifications were performed with pfu polymerase (Stratagene, La Jolla, CA, USA) at 55 °C annealing, 30 cycles.

In vitro transcription of α and β1 subunits was as described previously (Featherstone, Richmond & Ruben, 1996). RNA for both α and β1 subunits (1 : 1 volume, each at a concentration of about 1 μg μl^{-1}) was injected (50 nl oocyte^{-1}) into *Xenopus laevis* oocytes that were surgically removed from anaesthetized (0·17 % tricaine) frogs and separated using 2 mg ml^{-1} collagenase (Sigma), using standard methods previously described in detail (Featherstone *et al.* 1996; Richmond, Featherstone & Ruben, 1997). Before macropatch recording, vitelline membranes were manually removed following brief hyperosmotic treatment (Featherstone *et al.* 1996; Richmond *et al.* 1997).

All recordings were from oocytes injected with both α and β1 sodium channel subunits, using cell-attached macropatch techniques (Featherstone *et al.* 1996; Richmond *et al.* 1997), which allow excellent control of membrane voltage. Using macropatch methods, oocyte-expressed sodium channel kinetics (with or without co-expression of β1 subunit) always matched those measured from native channels or expressed in mammalian cell lines. Pipette solution used was (mM): NaCl, 96; KCl, 4; $MgCl_2$, 1; $CaCl_2$, 1·8; Hepes, 5; pH 7·4. Bath solution was (mM): NaCl, 9·6; KCl, 88; EGTA, 11; Hepes, 5; pH 7·4.

Voltage clamping and data acquisition were done as described previously (Featherstone *et al.* 1996; Richmond *et al.* 1997) using an EPC-9 patch-clamp amplifier (HEKA, Lambrecht, Germany) controlled via Pulse software (HEKA) running on a Power Macintosh 7100/80. All data were software low-pass filtered at 5 kHz during acquisition. The experimental bath temperature was maintained at 22 ± 0·2 °C for all experiments by using a peltier device controlled by an HCC-100A temperature controller (Dagan, Minneapolis, MN, USA). Where the voltage dependence of activation and/or inactivation was studied, the clamp control software (Pulse) alternated prepulse potentials, such that prepulse potentials were delivered as −160 mV, +10 mV, −155 mV, +5 mV, −150 mV, etc. if the voltage range of −160 to +10 mV was to be covered in 5 mV steps. The holding potential for all experiments was −120 to −150 mV, except for the action potential protocols in Fig. 4, which used a holding potential of −90 mV. Leak subtraction was performed automatically by the software using a *P*/4 protocol, except during the action potential-shaped waveform commands. Hardware leak–capacitance subtraction was done upon patch formation and corrected before each voltage clamp experiment, regardless of whether the experiment used rectangular or action potential command waveforms. The effect of leak during action potential protocols was minimized by using very tight seals (50–100 GΩ) and large currents. Action potential command waveforms were created initially as ASCII files in Igor Pro (Wavemetrics, Lake Oswego, OR, USA), loaded into Pulse as an ASCII 'buffer file', then saved in Pulse binary format for use by the pulse command generator. The initial ASCII files were created by attempting to duplicate, as closely as possible, the time course of rat muscle action potentials shown in Cannon, Brown & Corey (1993; Fig. 4*B* and *D*), minus any stimulus artifact.

Subsequent analysis and graphing were done using Pulsefit (HEKA) and Igor Pro (Wavemetrics), both run on a Power Macintosh 7100/80. All statistically derived values, both in the text and in figures, are given as means ± standard error of the mean (means ± S.E.M.).

Descriptions of test pulse inactivation rates and deactivation rates, given as time constants (τ), were derived from fitting the mono-exponential decay of individual test pulse or tail currents according to the function:

$$I(t) = \text{Offset} + a_1 \exp(-t/\tau),$$

where $I(t)$ is current amplitude as a function of time, Offset is the

plateau amplitude (asymptote), a_1 is the amplitude at time 0, and τ is the time constant (in ms). Time constants for the onset (and recovery) of inactivation were measured in the same way, except that fits were to peak current amplitude *vs.* prepulse (or interpulse) duration.

Steady-state activation and fast inactivation were fitted by a Boltzmann distribution, as follows:

$$\text{Normalized current amplitude} = 1/(1 + \exp(-ze_0(V_m - V_{½})/kT)),$$

where 'normalized current amplitude' is measured during a variable-voltage test pulse from a holding potential of −180 mV (for steady-state activation) or during a test pulse to 0 mV following a variable-voltage prepulse (for steady-state inactivation). V_m is the test pulse/prepulse potential, z is apparent valence, e_0 is the elementary charge, $V_{½}$ is the mid-point voltage, k is the Boltzmann constant, and T is absolute temperature.

Conductance (voltage) curves were computed using the equation:

$$G = I_{max}/(V_m - V_{rev}),$$

where G is conductance, I_{max} represents the peak test pulse current, V_m the test pulse voltage, and V_{rev} the measured reversal potential.

Muscle membrane simulations were performed using Simulation Control Program (SCoP) 3.5 (Simulation Resources Inc., Berrie Spring, MI, USA), using quantitative methods originally developed by Hodgkin & Huxley (1952) and subsequently adapted for mammalian skeletal muscle by Cannon *et al.* (1993). Briefly, simulated membrane potential changed as a result of combined ionic sodium, potassium and chloride (leak) currents. Sodium channel conductance was a function of m^3h gating, and potassium channel conductance a function of n^4 gating, where m, h and n parameters were assumed to obey first-order kinetics, as described in Hodgkin & Huxley (1952). The voltage dependence of the transitions of m, h and n were each defined by forward and backward rate constants following the formulations given as eqns (10), (11) and (12) in Cannon *et al.* (1993). In these equations, we used the gating parameters and conductances given in Table 1 of Cannon *et al.* (1993), which they used to successfully simulate human skeletal muscle excitability. Modified sodium channel fast inactivation and deactivation in paramyotonia congenita (this paper, Fig. 5*C–F*) was simulated by defining:

$$\text{Total } I_{Na} = (0{\cdot}5 I_{Na,WT}) + (0{\cdot}5 I_{Na,mutant}).$$

Thus, 50% of simulated channels were wild-type, and 50% were mutant, as occurs in the autosomal dominant disease. $I_{Na,WT}$ used normal gating parameters for rat and human skeletal muscle, as given in Cannon *et al.* (1993). $I_{Na,mutant}$ had fast inactivation recovery rates multiplied by 2, and fast inactivation onset rates multiplied by 0·25 (for Fig. 5*C* and *D*) and deactivation rates multiplied by 0·31 (for Fig. 5*E* and *F*). Forward and backward rates were adjusted for temperature according to a Q_{10} of 2·5. This Q_{10} was used for both wild-type and mutant channels.

RESULTS

The phenotype of paramyotonia congenita has been attributed to slowed fast inactivation, in combination with more rapid recovery from fast inactivation, compared with WT channels (Chahine, 1994; Yang *et al.* 1994; Hayward *et al.* 1996). Since the phenotype of the Arg→Pro substitution is more severe than that of the Arg→Cys substitution, we would therefore expect that R1441P should show the slowest inactivation kinetics and/or fastest recovery kinetics, compared with both R1441C and WT. We tested this hypothesis by measuring kinetics of fast inactivation onset and recovery, and show the results in Fig. 1.

Figure 1*A–C* shows representative groups of currents evoked by test pulses to varying potentials, for WT (Fig. 1*A*), R1441C (Fig. 1*B*) and R1441P (Fig. 1*C*). Both R1441C and R1441P had slower test pulse inactivation kinetics than WT. The time constants of these inactivation kinetics are plotted *versus* test pulse voltage in Fig. 1*D*. Inactivation time constants of both R1441C and R1441P were slower than WT at voltages between −50 and +40 mV, but R1441P and R1441C were identically slowed. In Fig. 1*E*, time constants of fast inactivation from closed states (filled symbols) and recovery from fast inactivation (open symbols) are plotted for voltages between −60 and −130 mV. As expected, R1441P and R1441C were faster to recover than WT, even at voltages as hyperpolarized as −130 mV. Potentials below −90 mV, muscle rest potential, are unlikely to be physiologically relevant. However, both R1441P and R1441C had identical recovery kinetics. The additional phenotypic severity of R1441P, therefore, cannot be completely explained by changes in fast inactivation.

Differences in hyperexcitability might be explained by differences in channel availability. To investigate this possibility, we measured the voltage dependence of activation and steady-state inactivation. These results are plotted in Fig. 2.

Figure 2*A* shows voltage dependence of activation for WT, R1441P and R1441C. At each test pulse voltage, about the same fraction of channels were activated for WT and the mutants. To ensure that all activatable channels were measured, this experiment was performed from a holding potential of −180 mV. Figure 2*B* shows the voltage dependence of steady-state inactivation. A prepulse of 500 ms was used, which is several times longer than needed to achieve steady-state in skeletal muscle sodium channels (Featherstone *et al.* 1996), but too short to induce slow inactivation (Featherstone *et al.* 1996). Test pulses (which measured the fraction of available channels) were to 0 mV. Significantly fewer channels were available for activation in both R1441P and R1441C, at potentials more negative than about −90 mV. Furthermore, the steady-state availability of both R1441P and R1441C channels was equivalent. Therefore, not only does steady-state inactivation not explain the severity of the R1441P phenotype, but these curves fail to predict the hyperexcitability of either mutant phenotype, since fewer R1441P or R1441C channels would be available at rest potential compared with WT.

A possibility that has not been considered as a cause for diseases of sodium channel hyperexcitability is slowed deactivation. In paramyotonia congenita, about half of the skeletal muscle sodium channels are WT, due to the autosomal dominant nature of the disease (Zhou *et al.* 1994). If only fast inactivation were slowed in mutant channels, it

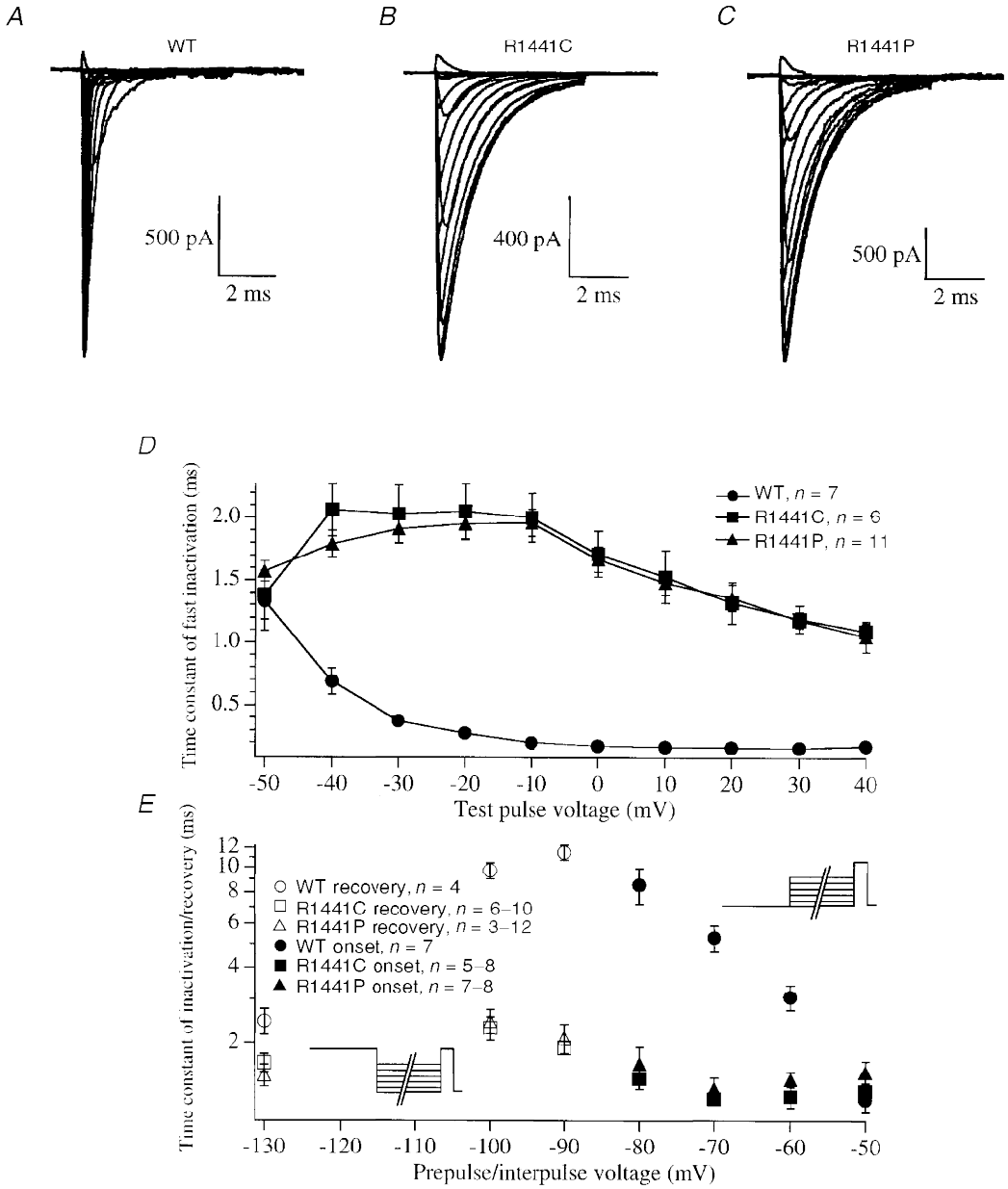

Figure 1. Rates of fast inactivation

A–C shows typical macropatch sodium currents evoked by test pulses from −180 mV to various potentials, for WT (*A*), R1441C (*B*), and R1441P (*C*) sodium channels, consisting of both α and $\beta 1$ subunits. Reversal potential was between +50 and +60 mV. Single exponentials were fitted to test pulse decay to derive the mean ± S.E.M. time constants for fast inactivation shown in *D*. *D* shows that fast inactivation in WT is faster than in both R1441P and R1441C, from −40 to +40 mV. However, inactivation time constants for R1441P and R1441C are not significantly different. In *E*, mean ± S.E.M. time constants for inactivation at −80 to −50 mV are plotted (filled symbols). These values were derived by fitting a single exponential to a plot of 0 mV test pulse amplitude *vs.* prepulse duration (see upper protocol diagram in *E*). *E* also shows mean ± S.E.M. time constants for fast inactivation recovery (open symbols). Recovery time constants were measured by fitting a single exponential to a plot of 0 mV test pulse amplitude *vs.* interpulse duration, where the interpulse followed a 500 ms step to 0 mV which fully inactivated all channels (see lower protocol diagram in *E*).

might be predicted that the normal inactivation of relatively fast-inactivating WT channels might still be sufficient to allow rapid repolarization of the membrane following an action potential. As a result of this rapid repolarization, mutant channels, even if they had not yet inactivated, might be closed by deactivation, and hyperexcitability might be therefore limited. If the mutant channels also had slowed deactivation, however, they would not close in response to the rapid repolarization, and a depolarizing sodium current would continue to flow, destabilizing the membrane potential. We therefore hypothesized that hyperexcitability might be exacerbated by slowed deactivation. Specifically, we predicted that deactivation in R1441P would be slower than deactivation in R1441C.

As a first step in testing this hypothesis, we measured tail current decay rates in WT, R1441P and R1441C. The results are shown in Fig. 3. Figure 3*A–D* shows typical tail currents at potentials from −120 to +20 mV (in 10 mV increments) following a short channel-opening step to +50 mV (see protocol diagram in Fig. 3*E*). Time constants from exponential fits to tail current decay are plotted in

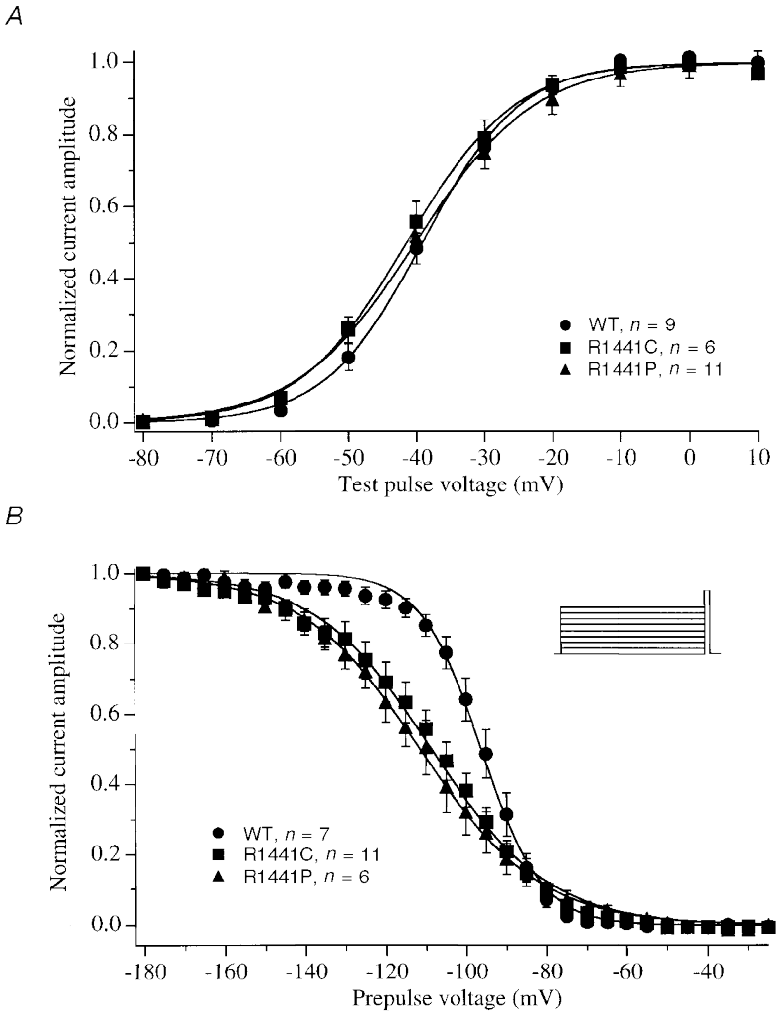

Figure 2. Voltage dependence of activation and fast inactivation

A shows the voltage dependence of activation for WT, R1441P and R1441C, as measured by the fraction of channels that open in response to a test pulse from −180 mV. A Boltzmann distribution has been fitted to each set of data, to yield the following fit coefficients: WT: $V_{½} = -39$ mV, $z = 3{\cdot}54$; R1441C: $V_{½} = -41$ mV, $z = 3{\cdot}19$; R1441P: $V_{½} = -40$ mV, $z = 2{\cdot}91$. *B* shows the voltage dependence of steady-state fast inactivation, as measured by the fraction of activatable (not inactivated) channels at 0 mV following a 500 ms prepulse to various potentials (see protocol diagram, top right). A Boltzmann distribution was fitted to each set of data, to yield the following coefficients: WT: $V_{½} = -96$ mV, $z = 3{\cdot}43$; R1441C: $V_{½} = -108$ mV, $z = 1{\cdot}76$; R1441P: $V_{½} = -111$ mV, $z = 1{\cdot}71$.

Fig. 3*E* (filled symbols, left vertical axis). Both R1441C and R1441P had slowed tail current kinetics, compared with WT. More importantly, tail current decay in R1441P was significantly slower ($P < 0{\cdot}01$, Student's t test) than that in R1441C, at all voltages between −110 and −20 mV (note the log vertical axis). We conclude from these data that deactivation in R1441P is slower than that in R1441C, and that both mutants' deactivation is slower than that of WT, as follows.

Tail current decay represents channel closings due to both inactivation and deactivation, where the amount of tail current decay due to deactivation increases as the membrane is repolarized to more negative potentials and the amount of tail current decay due to fast inactivation increases as the membrane is repolarized to more positive potentials. Although channels still close due to closed-state fast inactivation at negative potentials, the rate of deactivation is so much faster that tail current decay largely

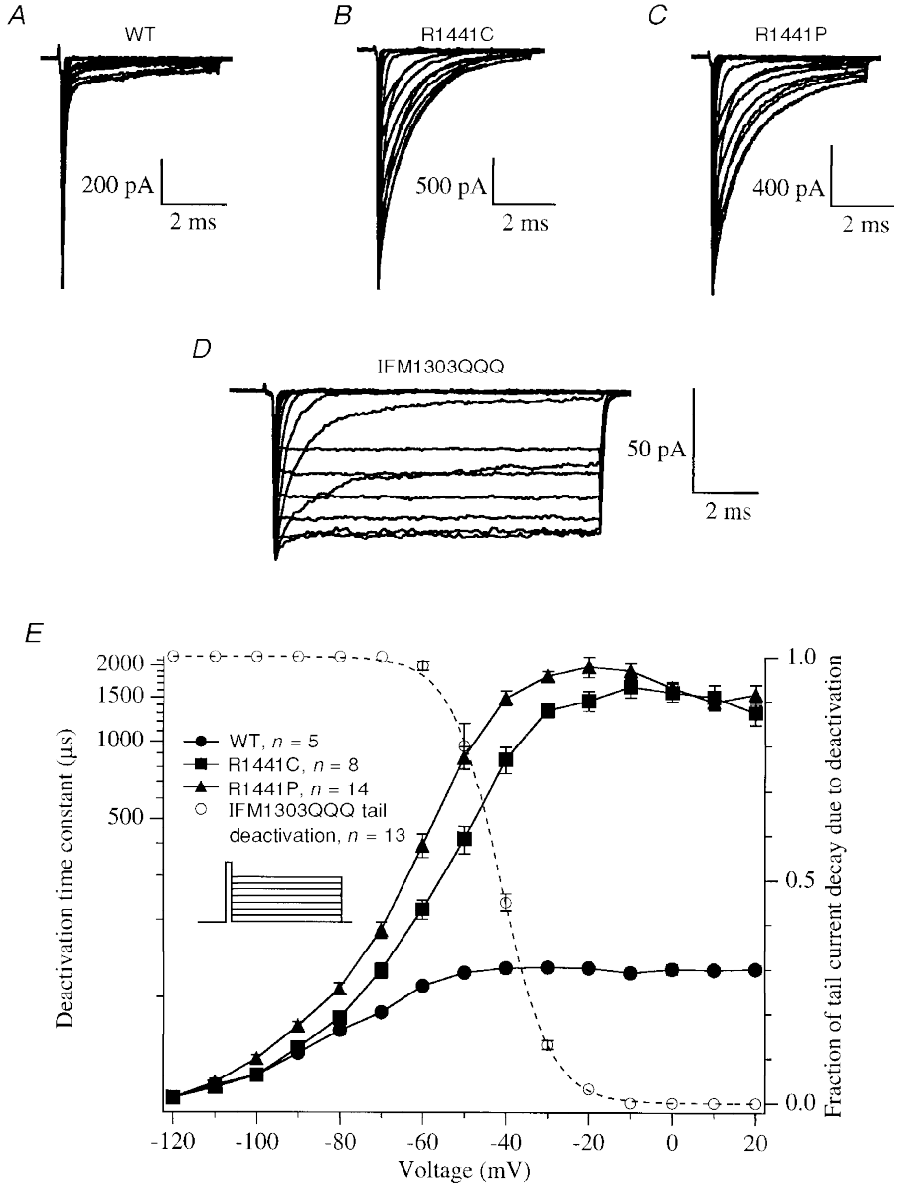

Figure 3. Tail current decay rates

A–D shows typical tail currents during a step to voltages from −120 to +20 mV, following a brief (0·5 ms), channel-opening pulse to +50 mV (see protocol diagram in *E*), for WT (*A*), R1441C (*B*), R1441P (*C*) and IFM1303QQQ (*D*). Single exponentials were fitted to tail current decays to derive the mean ± S.E.M. time constants plotted in *E* (filled symbols and lines, left vertical axis). The fraction of tail current that decayed (due to deactivation) in the fast inactivation-removed mutant IFM1303QQQ is also plotted in *E* (open circles, right vertical axis), and was fitted by a Boltzmann distribution (dashed line) with the following coefficients: $V_{½} = -41$ mV, $z = 4{\cdot}3$.

reflects deactivation. Following repolarization to more positive potentials, channels tend to stay activated rather than deactivate, and thus tail current decay reflects only fast inactivation. Therefore, the time constants shown in Fig. 3*E* are, depending on voltage, measures of rates of deactivation, fast inactivation, and mixed deactivation and fast inactivation.

However, the *difference* in tail current decay rates between R1441P and R1441C (Fig. 3*E*, squares and triangles) must be due to a difference in deactivation, rather than fast inactivation, for the following reasons: (1) fast inactivation rates for R1441P and R1441C were identical (see Fig. 1). Therefore, differences in R1441P and R1441C tail current decay must be due to differences in deactivation. (2) Tail current decay rates between −50 and −90 mV were *slower* in the mutants than in WT (Fig. 3*E*), while fast inactivation rates in this voltage range were *faster* (Fig. 1*E*).

Despite this strong evidence that deactivation is slower in R1441P than in R1441C (and both mutants have slower deactivation than WT), we further ensured that we were accurately interpreting tail current decay rate changes by obtaining tail current data from SkM1 channels wherein mutation of IFM1303QQQ selectively and completely removed fast inactivation at all voltages (West, Patton, Scheuer, Wang, Goldin & Catterall, 1992; Featherstone *et al.* 1996). With fast inactivation removed, tail current decay solely represents channel closings due to deactivation. IFM1303QQQ channels, however, are still probably entering a fast inactivated, but unblocked, conformation (Featherstone *et al.* 1996). Tail currents from SkM1 IFM1303QQQ are shown in Fig. 3*D*. The fraction of tail current that decayed in IFM1303QQQ is plotted against voltage in Fig. 3*E* (open circles, right vertical axis), and fitted with a Boltzmann distribution (dashed line). At −60 mV and more negative voltages, IFM1303QQQ tail currents decayed completely, indicating that tail decay rates at these voltages solely represent deactivation. More positive than about −20 mV, tail currents in IFM1303QQQ did not decay, showing that tail decay rates at these voltages (in WT or the PC mutants) represent fast inactivation. At −41 mV, tail current decay represents approximately equal amounts of deactivation and fast inactivation.

Above −20 mV, tail current decay rates for R1441P and R1441C were indistinguishable, in agreement with the finding (Fig. 1) that fast inactivation rates are identical for these two mutants. Tail current decay rates were, however, significantly different between R1441P and R1441C at potentials where we know (from the IFM1303QQQ data) that tail current decay is due mainly (−41 to −60 mV) or almost entirely (below −60 mV) to deactivation. This, in addition to the facts that fast inactivation in the mutants is identical, and fast inactivation in both mutants is faster

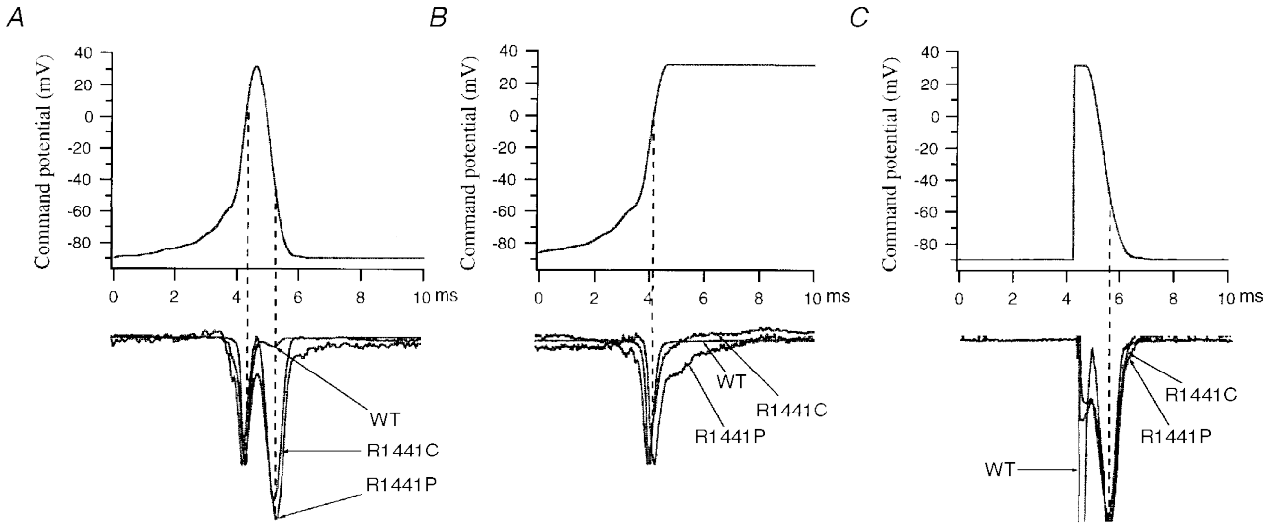

Figure 4. Sodium currents in response to action potential command waveforms

A, an action potential-shaped command potential was used to elicit sodium currents. *B*, the downstroke of the action potential command was eliminated. *C*, the action potential rise was replaced by a rectangular pulse to open channels, followed by an action potential 'downstroke'. A membrane voltage recording (reflecting the actual clamped voltage in the macropatch) is shown in the top panels of *A*–*C*. Typical WT, R1441C and R1441P sodium currents evoked by these protocols are shown below each voltage trace. A holding potential of −90 mV was used in order to mimic muscle fibre rest potential. Action potential waveforms (see Methods) were based on recordings from rat skeletal muscle shown in Cannon *et al.* (1993). No leak subtraction was used for any of the recordings shown, but seal resistances were 50–100 GΩ and sodium currents were large (several hundred picoamps). Dashed lines have been added to help compare timing of voltage and current recordings. Peak amplitude was normalized in each panel. Currents were normalized to size of the first peak in *A*, and second peak in *C*.

than WT below −50 mV, lead us to conclude that R1441P has slower deactivation than R1441C, and both mutants have much slower deactivation than WT.

Since only deactivation was different between R1441C and R1441P, slowed deactivation must be responsible for the more severe phenotype of the Arg→Pro mutation, consistent with the deactivation hypothesis outlined above.

In order for slowed deactivation to lead to hyperexcitability, however, action potential repolarization must be rapid enough that the fast rates of deactivation (hundreds of microseconds) must be physiologically relevant. To test this idea, and further examine the possible physiological behaviour of WT and mutant sodium channels, we used a voltage-clamp command potential in the shape of a skeletal muscle action potential (Cannon *et al.* 1993), and a holding potential of −90 mV, which is skeletal muscle rest potential (Ganong, 1995). Representative data from these experiments are shown in Fig. 4.

Figure 4*A* (upper panel) shows the voltage-clamp command waveform used to evoke the sodium currents shown beneath (Fig. 4*A*, lower panel). The sodium currents evoked by this command displayed two peaks: one occurring during the rising phase of the action potential, and the other during the falling phase of the action potential (dashed lines are shown to aid visual comparison of events). In the example shown in Fig. 4*A*, the sodium currents have been normalized so that the size of the first peak is identical. The size of the second sodium current peak (relative to the first) was always larger in the mutants, compared with WT, consistent with the idea that most WT sodium channels are inactivated before the falling phase of an action potential. Since the holding potential for these experiments was −90 mV (in order to approximate *in vivo* muscle rest potential), sodium channel availability was low (see Fig. 2*B*) and current amplitudes were relatively small compared with current sizes obtained in other experiments. For example, using mutant (R1441P and R1441C) channels, the first peak was typically only about 20–200 pA, while the second peak ranged from about 50 to 400 pA. WT amplitudes were about 150–800 pA for the first peak, and 30–250 pA for the second peak. Most of the variability in current amplitude occurred between oocytes, and patches within oocytes, presumably due to within- and between-oocyte variation in channel expression levels. We quantitatively compared the differences in second peak size by normalizing the size of the total current to the first peak amplitude (as in Fig. 4*A*, lower panel), then computing the area under the second peak. The ratios (R1441P peak 2 area)/(mean WT peak 2 area) and (R1441C peak 2 area)/(mean WT peak 2 area) were then computed, averaged, and compared using Student's *t* test.

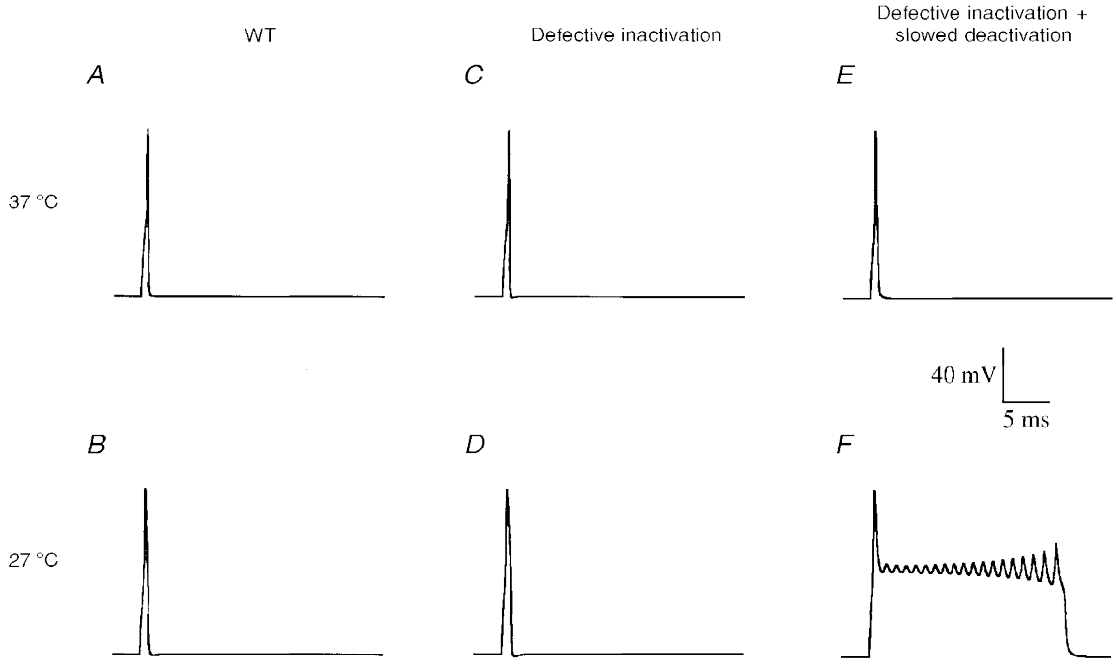

Figure 5. Simulations of paramyotonia congenita

A, a simulated membrane response (a single action potential) to a 0·5 ms 200 μA cm^{-2} stimulus, at 37 °C. *B*, the simulation was run under identical conditions except that a simulated temperature of 27 °C was used. In *C* and *D*, the simulation was repeated, except in this case fast inactivation recovery was accelerated twofold and fast inactivation onset slowed fourfold in 50 % of sodium channels in order to mimic previously reported defects in paramyotonia congenita. As in *A* and *B*, temperatures of 37 °C (*C*) and 27 °C (*D*) were simulated. In *E* and *F*, slowed deactivation has been added to the mutant fast inactivation simulated in *C* and *D*, in order to mimic the complete suite of defects we observed in this study.

The ratios were 8·88 ± 0·62 for R1441P, and 6·88 ± 0·52 for R1441C ($n = 8$, $P = 0·03$).

In order to test whether the first and second sodium current peaks were really due to the rise and fall, respectively, of the action potential, we created voltage command waveforms that consisted of only the rise (Fig. 4*B*, upper panel) or fall (Fig. 4*C*, upper panel) of an action potential. With the 'action potential rise' waveform, only the first peak occurred (Fig. 4*B*). This peak began at a voltage of about −60 mV, consistent with sodium channel activation, and decreased in size as the membrane approached the sodium current reversal potential (50–60 mV). We concluded that the first peak occurs as sodium channels open during the depolarization of an action potential.

With the 'action potential fall' waveform (Fig. 4*C*), a sodium current was elicited in response to the depolarizing step (initially needed to open channels), but the falling phase also evoked the second peak, as in the complete action potential-shaped waveform. The second peak amplitude was highly dependent upon the voltage to which the membrane was repolarized, and the steepness of the action potential waveform 'downstroke'. We concluded that the second sodium current peak is a tail current resulting not from a change in the number of open sodium channels, but a change in the driving force for sodium current. The second peak is physiologically important because this sodium current would oppose membrane repolarization following an action potential, and might therefore lead to hyperexcitability.

In a real action potential, the membrane voltage does not change in isolation from the currents it evokes, unlike the voltage clamp experiments shown here. Any sodium current flowing during the downstroke of an action potential would oppose repolarization. This opposition would slow the rate of repolarization, and consequently change the driving force for sodium. We used a computer simulation in order to explore the effects of slowed inactivation and deactivation in a dynamic membrane system, where current and voltage feedback loops are intact.

Figure 5 shows the results of muscle membrane simulations under different conditions. For the simulation (see Methods), standard Hodgkin–Huxley equations were used (Hodgkin & Huxley, 1952) to simulate sodium, potassium and leak (chloride) currents, with conductances, rates, concentrations, and Q_{10} values modified to match measurements from rat or human skeletal muscle, as reviewed in Table 1 of Cannon *et al.* (1993). In each of the panels (*A*–*F*) in Fig. 5, the membrane was stimulated with an identical short (0·5 ms) suprathreshold (200 μA cm^{-2}) stimulus in order to evoke an action potential. Figure 5*A*, *C* and *E* shows simulations at 37 °C. Figure 5*B*, *D* and *F* shows the same simulations run with the temperature parameter changed to 27 °C.

Figure 5*A* shows the results of simulating a muscle membrane containing WT sodium channels at 37 °C. In Fig. 5*B*, the simulation parameters are identical except that a temperature of 27 °C has been simulated. A temperature of 27 °C is cold enough to produce clinical myotonia in patients with paramyotonia congenita (Lehmann-Horn *et al.* 1987). In both Fig. 5*A* and *B*, only a single action potential was elicited in response to the stimulus. In Fig. 5*C* and *D*, fast inactivation onset has been slowed, and recovery from inactivation accelerated, in 50% of the simulated sodium channels in order to duplicate fast inactivation changes in the PC mutants. These conditions should mimic autosomal dominant paramyotonia congenita, wherein about half the channels are mutant (Zhou *et al.* 1994), assuming the only biophysical defect is that fast inactivation is slower and recovery faster, as has been previously reported for PC mutants (Chahine, 1994; Yang *et al.* 1994; Hayward *et al.* 1996). Figure 5*C* shows the simulation at 37 °C, and Fig. 5*D* shows results at 27 °C. In both cases, a single action potential was elicited by the stimulus.

In Fig. 5*E*, we show the results of simulations in which 50% of the sodium channels not only had modified fast inactivation, as in Fig. 5*C* and *D*, but also had deactivation slowed to match the difference between WT and the PC mutants. Figure 5*E* shows the simulation at 37 °C, where the stimulus resulted in a single action potential, as in Fig. 5*A*–*D*. Figure 5*F*, however, shows that a 10 degree lowering of temperature resulted in destabilization of membrane repolarization. This destabilization caused a prolonged 'burst' similar to 'myotonic runs' measured in paramyotonic human muscles (Rudel & Lehmann-Horn, 1985), and is consistent with the temperature-exacerbated inability of paramyotonia patients to relax muscles quickly after a contraction (Rudel & Lehmann-Horn, 1985; Wang *et al.* 1995*a*). The parameters used for Fig. 5*E* and *F* resulted in a model that was extremely sensitive to changes in both deactivation rate and temperature. A modest slowing of deactivation (as low as 1%) or lowering of temperature (a few degrees Celsius) resulted in burst duration increases of several tens of milliseconds, consistent with the temperature sensitivity and clinical severity of each mutation. In the model, myotonic runs result from the combined effects of modified fast inactivation and slowed deactivation, with deactivation rate being inversely correlated with the temperature at which myotonic runs occur and the severity (e.g. duration) of the myotonic burst. In other words, our simulations support the idea that the slowed deactivation in R1441P (compared with R1441C) results in hyperexcitability at higher temperatures, and myotonic bursts of longer duration, both consistent with the clinical phenotype of the equivalent human mutations.

In Fig. 6, the model parameters are identical to those used to generate Fig. 5*F*, except that sodium channel conductance for the simulated WT and mutant channels is shown. As in Fig. 5, the WT and mutant channels each make up 50% of the total channels in the simulation. Simulated WT channels activate, then quickly deactivate and/or inactivate in response to the suprathreshold stimulus and action potential. The continued depolarization (shown in Fig. 5*F*) results in a small amount (maximum conductance $< 0·03$) of

WT channel reactivation. Simulated mutant channels, however, fail to either inactivate or deactivate completely (conductance, 0·1–0·3) during the downstroke of the action potential, resulting in a 'persistent sodium current', and consequent failure of the membrane to repolarize, as shown in Fig. 5*F*.

These results are also consistent with simulations by Steinberg (1990) that did not study temperature effects, but showed that slowed deactivation and inactivation induce hyperexcitability in squid axons.

DISCUSSION

Slowed deactivation has heretofore not been considered as an underlying cause of paramyotonia congenita. In fact, physiologically important alterations in deactivation have not previously been observed. Our results, however, suggest that the clinical difference between patients with Arg→Pro and Arg→Cys mutations in skeletal muscle domain IVS4 may be due to a difference in sodium channel deactivation rates. Experiments with muscle action potential-shaped command potentials suggest that sodium current flows during the downstroke of an action potential, as a result of the fast change in driving force, and this action potential-evoked tail current is larger in paramyotonia mutants. Muscle membrane simulations show that the tail currents resulting from slowed inactivation and deactivation produce a temperature-sensitive destabilization of repolarization following an action potential. This destabilization results in 'myotonic runs' and predicts the phenotypic difficulty in muscle relaxation seen in paramyotonia congenita. With the exception of deactivation, which was not previously studied, our results are similar to those obtained from native WT and R1448P sodium channels in intact human skeletal muscle fibres (Lerche, Mitrovic, Dubowitz & Lehmann-Horn, 1996).

Previous work in our laboratory confirmed earlier studies showing that paramyotonia mutations T1313M and R1448C (the human equivalent of rat R1441C) had defects in fast inactivation, and narrowed the probable cause of the phenotype to slowed open-state fast inactivation (Richmond *et al.* 1997). Here, we modify that statement to suggest that a defect in fast inactivation alone does not adequately explain the disease. *In vivo* muscle repolarization involves multiple processes (Sperelakis, 1995): (1) activation of a delayed rectifier potassium current, (2) inward chloride currents, (3) sodium channel fast inactivation, and (4) sodium channel deactivation. Even if mutant sodium channels should fail to inactivate during an action potential, the repolarization (sustained by potassium and chloride conductances, and inactivation of WT sodium channels) would close sodium channels by deactivation, thereby terminating any depolarizing sodium current and minimizing hyperexcitability.

Therefore, we now suggest that myotonia may not result from slowed open-state fast inactivation *per se*, but rather that slowed fast inactivation enables mutant channels to remain open long enough (into the falling phase of an action potential) so that defects in deactivation become important. Mutant sodium channels neither close rapidly by themselves (inactivate), nor can be forced to close (deactivate) rapidly during an action potential, and this results in a current (the tail current/second peak in Fig. 4) proportional, but in opposition, to repolarization.

Modulation of ion channel deactivation may also be an important regulator of synaptic activity, since voltage-gated calcium channels have slow (relative to WT sodium channels) inactivation kinetics. Calcium influx has been shown to occur during the downstroke of presynaptic terminal action potentials as 'tail currents' (Borst & Sakmann, 1996).

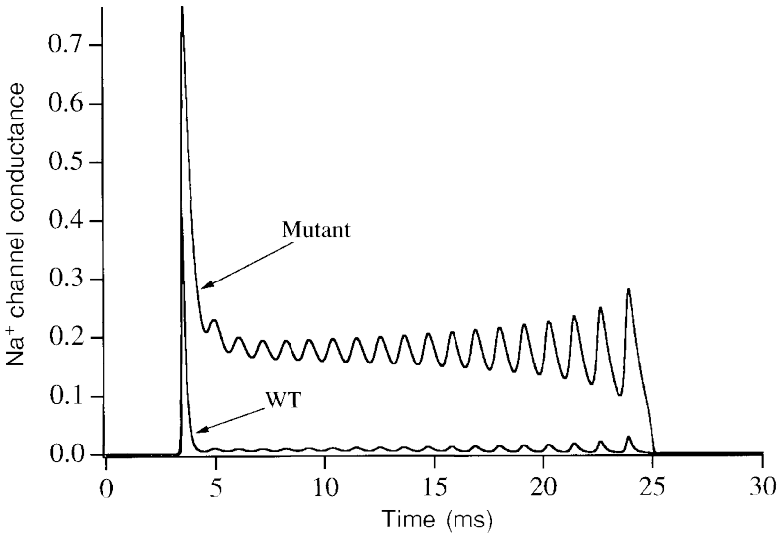

Figure 6. Conductance of simulated sodium channels underlying membrane voltage simulations in Fig. 5*F*

All parameters are identical to those used for Fig. 5*F*, except sodium conductance, rather than membrane voltage, is shown for the simulated WT and mutant channels.

In addition to the point that slowed deactivation rates can cause hyperexcitability consistent with PC, our simulations also argue that slowed deactivation helps explain the temperature sensitivity of the disease, which has not otherwise been convincingly accounted for. As the muscle temperature decreases, deactivation slows. A 'threshold' for symptoms is reached when deactivation takes longer than the membrane repolarization of an action potential. At this point, sodium channels cannot be deactivated fast enough to avoid a depolarizing sodium tail current, resulting in resistance to repolarization. Note that no unusual Q_{10} is required for mutant channel deactivation; the temperature dependence of hyperexcitability is a consequence of normal slowing of channel kinetics with cooling, relative to the flow of ionic current (which also slows with cooling, but less dramatically). The clinical temperature sensitivity of the Arg→Pro and Arg→Cys mutations is consistent with this hypothesis, in that Arg→Pro, with the slowest deactivation, has the greatest temperature sensitivity (Wang *et al.* 1995*a*). Furthermore, slowed deactivation has not only been measured in the S4 voltage sensor mutations described here, but also in two other temperature-sensitive myotonia mutations: T1313M and G1306E (Hayward *et al.* 1996). Slowed deactivation may therefore be an important characteristic shared by the temperature-sensitive mutant sodium channel myotonias, and further investigation may reveal that this property separates PC from related phenotypes.

The simulations in Figs 5 and 6 used Hodgkin–Huxley (HH) type sodium channels to demonstrate quantitatively, using the simplest possible realistic model, that a combination of slowed sodium channel deactivation and fast inactivation is capable of producing repetitive muscle membrane firing similar to that seen in real myotonia. The HH sodium channel model, however, is not consistent with the structural implications of our data. In particular, the fact that we see slowed deactivation without apparent shifts in the rate or voltage dependence of activation (as did Ji, George, Horn & Barchi (1996) in hSkM1 R1448C) may not be consistent with activation and deactivation being inverse directions of a symmetrical first-order conformational change.

Rayner, Starkus & Ruben (1993) have shown that sodium channel activation requires a voltage-insensitive, solvent-sensitive hydration step immediately prior to opening, whereas deactivation does not; therefore activation and deactivation occur via different pathways. Starkus, Schlief, Rayner & Heinemann (1995) have proposed a solvent-sensitive activation gating model for *Shaker* potassium channels which may also be applicable to sodium channels. Briefly, their model assumes that tetrameric potassium channels can exist in two quaternary conformations, 'tense' (non-openable) and 'relaxed' (potentially openable), and each monomer can be either 'activated' or 'deactivated' regardless of tense–relaxed conformation. Channel opening requires activation of all four monomers in addition to a solvent-sensitive shift from the tense (T) to relaxed (R) conformation. The probability of a T–R transition increases co-operatively with activation of more monomers. Deactivation, however, requires only movement of one monomer, without a shift from relaxed to tense conformations. Unlike tetrameric potassium channels, sodium channel domains may gate in a preferred order. If charge deletions in DIVS4 (like rSkM1 R1441C/P or hSkM1 R1448C) preferentially affect deactivation (compared with charge deletions in other domains), then deactivation in DIVS4 charge deletion mutants may be slowed because movement of the now 'crippled' DIVS4 is the first step in deactivation, or the S4 movement order changes such that movement of relatively slower S4s in domains I–III are now rate limiting.

The Starkus *et al.* (1995) model does not include inactivation. However, an attractive model of sodium channel inactivation has been proposed by Kuo & Bean (1994). This model suggests that the probability of fast inactivation increases co-operatively as each sodium channel domain activates, and conversely, recovery from inactivation probability increases as each domain deactivates, such that recovery from fast inactivation in sodium channels tends to follow deactivation. Slowed deactivation should then result in slowed recovery from fast inactivation. But recovery from inactivation in our R1441P/C mutants, as well as in hSkM1 R1448C (Ji *et al.* 1996) is faster, despite slowed deactivation. A possibility is that the DIVS4 outer charge mutants only affect deactivation from non-inactivated states. Kuo–Bean type fast inactivation could be appended to the Starkus *et al.* (1995) model by assuming that fast inactivation occurs only from the 'relaxed' conformation. Experiments designed to develop and test such a model are in progress.

Bennett, P. B., Yazawa, K., Makita, N. & George, A. L. Jr (1995). Molecular mechanism for an inherited cardiac arrythmia. *Nature* **376**, 683–685.

Borst, J. G. G. & Sakmann, B. (1996). Calcium influx and transmitter release in a fast CNS synapse. *Nature* **383**, 431–434.

Cannon, S. C. (1996). Ion-channel defects and aberrant excitability in myotonia and periodic paralysis. *Trends in Neurosciences* **19**, 3–10.

Cannon, S. C., Brown, R. H, & Corey, D. P. (1993). Theoretical reconstruction of myotonia and paralysis caused by incomplete inactivation of sodium channels. *Biophysical Journal* **65**, 270–288.

Chahine, M. (1994). Sodium channel mutations in paramyotonia congenita destabilize inactivations. *Neuron* **12**, 1–20.

Featherstone, D. E., Fujimoto, E. & Ruben, P. C. (1997). Slowed sodium channel deactivation exacerbates hyperexcitability in paramyotonia congenita. *Biophysical Journal* **72**, A116.

Featherstone, D. E., Richmond, J. E. & Ruben, P. C. (1996). Interaction between fast and slow inactivation in Skm1 sodium channels. *Biophysical Journal* **71**, 3098–3109.

Ganong, W. F. (1995). *Review of Medical Physiology.* Appleton & Lange, Norwalk, CT, USA.

George, A. L., Komisarof, J., Kallen, R. G. & Barchi, R. L. (1992). Primary structure of the adult human skeletal muscle voltage-dependent sodium channel. *Annals of Neurology* **17**, 131–137.

Hayward, L. L., Brown, R. H. Jr & Cannon, S. C. (1996). Inactivation defects caused by myotonia-associated mutations in the sodium channel III–IV linker. *Journal of General Physiology* **107**, 559–576.

Ho, H. N., Hunt, H. D., Morton, R. M., Pullen, J. K. & Pease, L. R. (1989). Site-directed mutagenesis by overlap extension using the polymerase chain reaction. *Gene* **77**, 51–59.

Hodgkin, A. L. & Huxley, A. F. (1952). A quantitative description of the membrane current and its application to conduction and excitation in nerve. *Journal of Physiology* **117**, 500–544.

Ji, S., George, A. L. Jr, Horn, R. & Barchi, R. L. (1996). Paramyotonia congenita mutations reveal different roles for segments S3 and S4 of domain D4 in hSkM1 sodium channel gating. *Journal of General Physiology* **107**, 183–194.

Kuo, C. & Bean, B. P. (1994). Na^+ channels must deactivate to recover from inactivation. *Neuron* **12**, 819–829.

Lehmann-Horn, F., Rudel, R. & Ricker, K. (1987). Membrane defects in paramyotonia congenita (Eulenburg). *Muscle and Nerve* **10**, 633–641.

Lerche, H., Mitrovic, N., Dubowitz, V. & Lehmann-Horn, F. (1996). Paramyotonia congenita: the R1448P Na^+ channel mutation in adult human skeletal muscle. *Annals of Neurology* **39**, 599–608.

Ptacek, L. & Griggs, R. C. (1996). Familial periodic paralysis. In *Molecular Biology Membrane Transport Disorders*, pp. 625–642. Plenum Press, New York.

Rayner, M. D., Starkus, J. G. & Ruben, P. C. (1993). Hydration forces in channel gating. *Comments in Molecular and Cellular Biophysics* **8**, 155–187.

Richmond, J. E., Featherstone, D. E. & Ruben, P. C. (1997). Paramyotonia congenita results from defects in Na^+ channel fast, but not slow inactivation. *Journal of Physiology* **499**, 589–600.

Rudel, R. & Lehmann-Horn, F. (1985). Membrane changes in cells from myotonia patients. *Physiological Reviews* **65**, 310–356.

Sansone, V., Rotondo, G., Ptacek, L. J. & Meola, G. (1994). Mutation in the segment of the adult skeletal sodium channel gene in an Italian paramyotonia congenita (PC) family. *Italian Journal of the Neurological Sciences* **15**, 473–480.

Schwartz, P. J., Priori, S. G., Locati, E. H., Napolitano, C., Cantu, F., Towbin, J. A., Keating, M. T., Hammoude, H., Brown, A. M., Chen, L. S. K. & Colatsky, T. J. (1995). Long QT syndrome patients with mutations of the SCN5A and HERG genes have differential responses to Na^+ channel blockade and to increases in heart rate: Implications for gene-specific therapy. *Circulation* **92**, 3381–3386.

Sperelakis, N. (1995). Electrogenesis of membrane excitability. In *Cell Physiology Source Book*, pp. 255–278. Academic Press, Inc., San Diego, CA, USA.

Starkus, J. G., Schlief, T., Rayner, M. D. & Heinemann, S. H. (1995). Unilateral exposure of *Shaker* B potassium channels to hyperosmolar solutions. *Biophysical Journal* **69**, 860–872.

Steinberg, I. Z. (1990). Computer simulations of electrical bistability in excitable cells due to non-inactivating sodium channels: space- and time-dependent behavior. *Journal of Theoretical Biology* **144**, 75–92.

Trimmer, J. S., Cooperman, S. S., Tomiko, S. A., Zhou, J., Crean, S. M., Boyle, M. B., Kallen, R. G., Sheng, Z., Barchi, R. L., Sigworth, F. J., Goodman, R. H., Agnew, W. S. & Mandel, G. (1989). Primary structure and functional expression of a mammalian skeletal muscle sodium channel. *Neuron* **3**, 33–49.

Wang, J., Dubowitz, V., Lehmann-Horn, F., Ricker, K., Ptacek, L. & Hoffman, E. P. (1995*a*). *In vivo* channel structure/function studies: consecutive Arg1448 changes to Cys, His, and Pro at the extracellular surface of IVS4. In *Ion Channels and Genetic Diseases*, pp. 77–88. Rockefeller University Press, New York.

Wang, Q., Shen, J., Splawski, I., Robinson, J. L., Moss, A. J., Towbin, J. A. & Keating, M. T. (1995*b*). SCN5A mutations associated with an inherited cardiac arrhythmia, long QT syndrome. *Cell* **80**, 805–811.

West, J. W., Patton, D. E., Scheuer, T., Wang, Y., Goldin, A. L. & Catterall, W. A. (1992). A cluster of hydrophobic amino acids residues required for fast Na^+ channel inactivation. *Proceedings of the National Academy of Sciences of the USA* **89**, 10910–10914.

Yang, N., Ji, S., Zhou, M., Ptacek, L. J., Barchi, R. L., Horn, R. & George, A. L. Jr (1994). Sodium channel mutations in paramyotonia congenita exhibit similar biophysical phenotypes *in vitro*. *Proceedings of the National Academy of Sciences of the USA* **91**, 12785–12789.

Zhou, J., Spier, S. J. & Hoffman, E. P. (1994). Pathophysiology of sodium channelopathies: correlation of normal/mutant mRNA ratios with clinical phenotype in dominantly inherited periodic paralysis. *Human Molecular Genetics* **3**, 1599–1603.

Acknowledgements

The authors would like to thank Dr Janet Richmond, Dr Robert Ruff and Jennifer Abbruzzese for critical reading of this manuscript and Dr Martin Rayner for helpful discussion. This work was supported by PHS grant R-01 NS29204 and a Muscular Dystrophy Association grant to P.C.R.

Corresponding author

D. E. Featherstone: Department of Biology, University of Utah, Salt Lake City, UT 84112, USA.

Email: featherstone@biology.utah.edu